EXPERIMENTAL INVESTIGATION OF CRACKING LOCALIZATION IN RC BEAMS WITH STEEL FIBERS

Yosef Yaynishet Gebreyesus[1] Yuri S Karinski[2*], Avraham N. Dancygier[1,2] and Marco di Prisco[3]

[1] Faculty of Civil and Environmental Engineering, Technion – Israel Institute of Technology
[2] National Building Research Institute, Technion – Israel Institute of Technology
[3] Department of Civil and Environmental Engineering, Politecnico di Milano

Abstract

This paper presents an experimental study aimed to identify and quantify the cracking localization (CL) phenomenon in under-reinforced R/SFRC beams. Results of current experiments together with those of previous tests published by the authors were used for quantification of the cracking localization level (CLL) considering the effect of fiber content, V_f, and of longitudinal reinforcement ratio, ρ_s, over a wide range of ρ_s and the effect of rebar yield and ultimate strengths. The experimental program consisted of four-point bending tests of normal strength R/SFRC beam specimens with 400 and 500-MPa steel and fiber volumetric contents V_f of 0.5 and 0.76%. A new definition is introduced for 'significantly wide cracks' that yields a unique definition of the CLL when this phenomenon diminishes. Moreover, it is now proposed to change the definition of CLL. The study identified the existence of a transition point (TP), beyond which addition of fibers to the concrete mix do not affect CLL anymore. Observations from the experimental results prove the consistency of the newly proposed CLL definitions as well as the dependency of CL on both the amount and stress hardening of the tension steel. Their use enables a clear delineation of the cracking localization phenomenon in R/SFRC beams. The importance of this finding refers to the reported decrease of flexural ductility in R/SFRC beams due to high CLL. Hence, the importance of the ability, achieved in the current findings, to quantify the conditions for TP's in various cases.

KEYWORDS
Crack localization; Fiber reinforced concrete; Bending tests; FRC classification

* Corresponding author. Tel. +972-4-8293187; E-mail: karinki@technion.ac.il

1 INTRODUCTION

Steel fibers are used in combination with conventional reinforcement in structural members such as slabs and beams to improve cracking behavior and ductility. Indeed, fibers improve the material cracking behavior under serviceability load and its ultimate flexural ductility for beams containing higher conventional reinforcement ratios (e.g., Model Code 2010[1]). However, addition of fibers can cause also cracking localization (CL), which occurs in reinforced concrete (RC) tension[2-4] and flexural[5-7] elements with relatively low reinforcement ratios, that include steel fibers (R/SFRC elements). Earlier works on CL are mentioned in Markic et al.[32]. This phenomenon is characterized by significant opening of one or few cracks under the ultimate load, out of all cracks that develop prior to yielding of the tension steel[4,8-10]. In R/SFRC beams this strain localization leads to decrease of their flexural ductility[11,12] for both normal[11,13] and high[6,11] strength concrete.

CL has been explained by the non-uniform distribution of the fibers along the R/SFRC element[14,15], considering also the fibers effectiveness (including the fibers orientation[16-19]). This non-uniform distribution leads to existence of so-called "weak segments"[20] where the fibers effectiveness is relatively low, compared with its mean value along the structural element.

This phenomenon leads to strain localization within the wide cracks, which significantly strains the steel rebars that bridge these cracks[11,20]. It has also been shown that for a given conventional reinforcement ratio, cracking localization is more pronounced for larger fiber contents[4,21].

Test results showed that CL level in R/SFRC beams is most pronounced with low conventional reinforcement ratios, ρ_s. When ρ_s increases CL decreases and beyond a certain level of ρ_s it diminishes[3,20]. Moreover, it has been observed that there exist two distinct ranges of ρ_s within which the decreasing gradients of CL are significantly different: for the range of low ρ_s the gradient is much steeper than it is within the second range[4,11]. The point that marks the changeover from the first to the second range has been denoted in[22] "transition point" (TP). The experiments also show that for a given ρ_s when the fibers volumetric content V_f increases CL increases as well[4]. According to other researchers, there exits also a transition point that refers to other aspects related to CL[12].

Yet, studies of CL still show knowledge gaps, mainly in two aspects, namely, quantification of the CL level and of the TP (as explained in more details in the following text). Furthermore, the literature refers to a possible influence of the conventional steel mechanical properties on CL only rarely[23] and hardly ever - on the TP.

The study reported in this paper aimed to experimentally identify and quantify the CL level and the TP, depending on the conventional reinforcement ratio, the fibers content and on the stress hardening of the conventional reinforcement.

2 CL NEW DEFINITION AND RESEARCH OBJECTIVES

Papers previously published by the authors[4,11] defined the crack localization level (CLL) in terms of the ratio between the number of the 'significantly wide cracks', '**m**', and the total number of cracks, '**n**'. Thus, for **n** > 1, when there is a single wide crack, **m**=1, there is a high level of crack localization. As **m** increases (for the same number **n**) CLL decreases, where for **m** approaching **n** CLL diminishes. These papers defined 'significantly wide cracks' as those whose width was larger than the others by an order of magnitude or more (about 10 times wider). All the cracks within the constant moment zone were examined at the end of the test. However, the definition of CLL in terms of **m**/**n** raises the question regarding the case of large ρ_s/V_f ratio for which all crack widths are similar (at the ultimate limit state, ULS). On the one hand there are no 'significantly wide cracks' and **m** is apparently equal to 0, and on the other hand all cracks may be referred to as 'wide cracks', i.e., **m** = **n**.

Note that it has been observed that prior to yielding of the tension steel, all cracks (under the same moment) had similar widths. After yielding and up to ULS, in plain RC beams, these cracks widen significantly, more-or-less uniformly. In contrary, in R/SFRC beams only part of these cracks widen significantly (depending on ρ_s/V_f) while widths of the other cracks hardly increase.

Therefore, here we introduce the following new definition: 'significantly wide cracks' are those whose width at the end of the test is larger by an order of magnitude or more, than the average width of cracks *just before yielding* of the tension steel. According to this definition, the case of uniform crack widening at ULS corresponds uniquely to **m** = **n**.

Moreover, it is now proposed to change the definition of CLL and to use the ratio **n/m** (rather than **m/n**) to quantify it, such that **n/m** and CLL will now have the same trends. I.e., when **n/m** increases CLL increases as well and vice versa.

The previous papers also pointed out the lack of results with relatively low fiber contents (< 0.76%). Furthermore, these tests did not provide enough information for a certain range of ρ_s, in order to identify the transition point discussed in the introduction. Additionally, the previous tests were performed with mostly deformed rebars of 400-MPa yield strength.

To answer the questions raised above, the current work presents an extended series of flexural experiments of R/SFRC beams. Results of the current experiments together with those of the tests described above were used for quantification of CLL according to the new definition, considering:

i. The effect of fiber content, V_f, and of longitudinal reinforcement ratio, ρ_s, over a wide range of ρ_s.
ii. The effect of rebar yield and ultimate strengths.

Additionally, these results yield the identification of a transition point.

3 EXPERIMENTAL PROGRAM

The experimental program consisted of four-point bending tests of normal strength R/SFRC beam specimens with hooked-end steel fibers. The beams had a cross-section of 240x300-mm^2 (width x height), and a span of 3.2 m with a 1.5-m constant moment zone (Figure 1). All the specimens had two-8mm steel rebars in the compression zone and they were also provided with 10-mm stirrups all along their length, with an adequate amount given in the shear span to avoid shear failure (spacing of the stirrups were 215 mm in the constant moment zone for all specimens and in the shear span, as follows: 175 for ρ_s = 0.53%, 150 for ρ_s = 0.63 and 0.72% and 125 for ρ_s = 0.94 and 1.26%). The cover from the bottom and top sides was 15 mm, while 20 mm was their cover from both sides, as shown in Figure 1.

The previous test series[11] included 8 specimen types (see Table 1) with deformed rebars of 400-MPa nominal yield strength (except for one type of specimens with ρ_s = 0.15% which had 500-MPa steel). The current program comprised seven specimen types (Table 1), with deformed rebars of 500-MPa nominal yield strength (except for one type of specimens with ρ_s = 0.72% which were 400-MPa steel).

In both test series two specimens of each type were tested. When results of the two tested beams appeared to vary significantly an additional specimen was cast and tested (denoted by "3" as the last character in specimen notation, Table 1).

The differences between the specimen types were the fiber and conventional reinforcement contents. The fiber contents that were applied were 0.5% and 0.76% in volume, which correspond to fiber weights of 40 and 60 kg/m^3, respectively. The conventional reinforcement ratios ranged from 0.15% to 3.3% as detailed in Table 1. The rebars stress-strain curves are given in Appendix A.

The load was applied until failure using deflection-control of the testing machine piston at a rate ranging from 0.25 to 3-mm/min. The slower rates of the piston were applied from the start of the loading up to at least post-yielding of the tension steel rebars. Cracks formed in the constant moment zone were carefully marked and monitored manually during the test until yielding of the tension steel was reached and their number was denoted **‘n’**. Yielding was identified when starting of load-deflection plateau was observed. At the end of the test, the cracks were examined to identify those that widened significantly more than the others and their number was denoted **'m'**.

4 MATERIALS

The conventional reinforcement consisted of standard deformed bars, detailed in Table 1. The rebars relevant properties (see also following section), i.e., yield and maximum strengths, for both test series (present and previous[11]) are given in Table 1.

One type of 3D Hooked-end fibers was used in the concrete mixes in both previous and current tests. The fibers had 35-mm length and a diameter of 0.55 mm with an aspect ratio of 64 (Dramix RC-65/35-BN[24]).

The concrete mix was designated to be normal strength concrete with nominal compressive strength of 30 MPa. Portland cement CEM I-52.5N with dolomite aggregate of 19 mm maximum size were used. The mix components and proportions are presented in Table 2.

Mean compressive strengths of the specimens are given in Table 1. The fibrous concrete cast in the current series was classified as per prEN 1992-1-1 2021 Annex C(7)[25], MC2010[1,26] and EN 14651[27], by three-point bending tests of notched 150x150x550-mm beams: three days prior to their testing date, the beams were wet-sawn to a depth of 25-mm with a width of 5 mm, forming a notch at the middle, rotated 90^{o} relative to the longitudinal axis and parallel to the casting direction. After sawn in wet, they were returned to the water for two days. Three to four specimens were tested for each batch at 29 days or later (see Table 3). Classification was done for all specimens of the two types of mixtures, with 40 and 60 kg/m^3 of fibers, without differentiating between their casting batches (according to the above codes a minimum of 6 specimens are required for each mixture).

The residual flexural tensile strength, denoted $f_{R,i}$ (i=1,2,3,4), used for characterization and classification of the SFRC composite, were calculated from the measured load vs CMOD (crack mouth opening displacement). Figures of load-CMOD curves, from which these data were obtained, are shown in Appendix B. As prescribed in the above codes the FRC classification is based on two parameters: residual strength f_{R1k}, and the f_{R3k}/f_{R1k} ratio. The measured f_{r1} and f_{r3} values, used for the calculation, are shown in Table 3.

The characteristic values f_{r1k} and f_{r3k} are calculated as follows[25,28,29]:

- Calculate the average value, f_{rim}, standard deviation, σ_{rim} (of the data in each row in Table 3) and the coefficient of variation, $CoV_i = \sigma_{rim} / f_{rim}$.
- Calculate the log-normal average[29] in the following way:

$$f_{ri,ln} = e^{(m_{yi} - k_n \cdot s_{yi})},\ i = 1,3 \tag{1}$$

where

$$m_{yi} = \frac{\sum ln(f_{ri})}{n},\ s_y = \sqrt{ln(CoV_i^2 + 1)}, \tag{2}$$

n is the number of specimens and k_n is obtained according to n from Table D1 in EN 1990[29].

- The final value of $f_{ri,k}$ is determined according to prEN 1992-1-1[25] as follows:

$$f_{ri,k} = MIN\{0.6 f_{rim}, f_{ri,ln}\} \tag{3}$$

The class of the mixture is described by a number and a letter. The number corresponds to the "residual strength class" (RSC) which is defined by the residual flexural strength $f_{R,1k}$ (Eq. (3)) down-rounded according to the following sequence of numbers[25]: 1.0; 1.5; 2.0; 2.5; 3.0; 4.0; 5.0; 6.0; 8.0. The latter is set by the interval in which the f_{R3k}/RSC ratio falls, as defined in[1,30]. In the following the letter is denoted "ratio-based class" (RBC). For example, a FRC mix that has a strength $f_{R1}k$ of 3.7 MPa and a f_{R3k}/RSC ratio that falls within 0.7 and 0.9 will have a class of 3b (RSC = 3 and RBC = b).

The resulted calculations and the classifications of the two mixes that were used in this study are given in Table 4.

Both mixtures have the same RBC ("d") while their RSC are different, where the larger value relates to the mixture with the larger fiber content ("3" vs. "2.5").

5 RESULTS - QUANTIFICATION OF CRACK LOCALIZATION

Figure 2 shows a typical beam specimen just after yielding, where all the cracks have widths of the same order. Figure 3 shows three cases of beams at the end of the test with different numbers of significantly wide cracks (i.e., with different CLL).

All cracks that formed prior to yielding of the tension steel had similar widths that did not exceed 0.4 mm. These cracks were counted, and their number is denoted '**n**'. The significantly widened cracks developed only after yielding and only within the constant moment zone. These cracks were counted at the end of the test, and their number is denoted '**m**'. Counting of the flexural cracks was done on both sides of each beam and their numbers were averaged for the subsequent analysis. This data is summarized in Table 5 for both test series, previous and current. It is important to note that while samples tested in these series had the same geometric characteristics (setup, cross-sectional dimension, span, shear span and constant moment zone) the mechanical properties of the tension rebars were different, as detailed in Table 1. For this reason, their ratio of maximum-to-yield stresses f_u/f_y is also given in Table 5.

The main observations from the experimental results given in Table 5 are the following:

- Few cracks widened significantly in specimens with low longitudinal reinforcement ratios. For example, for R/SFRC beams with a longitudinal reinforcement ratio of

0.15% and fiber content of 0.5%, only 1-2 cracks widened significantly out of a total of 10-12 cracks, yielding **n/m** = 6 - 10.

- Upon increasing the reinforcement ratio, but keeping the same fiber content (0.5%), the number of significantly widened cracks, **m**, increased. For example, for ρ_s = 0.53% **m** = 5 - 5.5 out of **n** = 17 - 17.5, yielding **n/m** = 3.18 - 3.40.
- For the same fiber content, but much larger ρ_s of 1.26% **n/m** = 1.38 - 1.52, which indicates diminishing of the cracking localization phenomenon.
- A similar trend of CLL variation with ρ_s was observed for the specimens with a fiber content of 0.76%.

Figure 4 shows CLL values (in terms of the ratios **n**/**m**) depending on the conventional reinforcement ratio ρ_s. The graphs show all measured data points as well as their averages for each value of ρ_s.

The figure shows that there is a larger scatter of **n**/**m** for lower values of ρ_s: when ρ_s is more than 0.39 and 0.53% for V_f of 0.5 and 0.76%, respectively, the scatter is negligible.

It is evident from Figure 4 that for both fiber contents there exists a transition point (TP), after which **n**/**m** ratios are hardly affected by the reinforcement ratio. This observation is further presented in Figure 5a by plotting linear trendlines according to all measured data points, whose intersections indicate these TPs in terms of ρ_s (Figure 5b).

It is noted that for plain concrete (V_f = 0) there is no crack localization and therefore, as the fibers content decreases, the TP coordinates should decrease as well (no effect of ρ_s on CLL). Yet, the results plotted in Figure 5b do not conform to this trend. According to the trendlines, for V_f = 0.5% the TP value of ρ_s is 0.70% while for V_f = 0.76% it is 0.69%. Although these values are close, they indicate a trend opposite to the one described above.

This unexpected result may be explained by the use of different types of steel (see Table 1), as follows. It has been shown that because of the non-uniform fiber distribution along the beam, 'significantly wide cracks' develop in "weak cross-sections", where there is relatively low effectiveness of the fibers[12,14,15]. It is also noted that widening of a crack depends on the elongation and slip of the tension rebars that bridge this crack. CL starts when the tensile steel starts to yield, where elongation of the bridging rebars occurs and therefore, the crack widening of particular cracks depends on the post-plateau hardening rate of the bridging steel. Thus, a larger hardening rate can inhibit significant widening of some of these cracks.

The steel hardening rate can be characterized by the ratio of the maximum-to-yielding stresses, f_u/f_y. Therefore, the following new parameter is introduced, which considers both the amount and hardening of the conventional reinforcement:

$$\rho_{eff} = \rho_s \cdot f_u/f_y \quad (4)$$

The above measured CLL data depending on this parameter (ρ_{eff}) are shown in Figure 6. Figure 6b shows that according to the new parameter, for V_f = 0.5% the TP value of ρ_{eff} is 0.0094 (point A in the figure) while for V_f = 0.76% it is 0.0099 (point B). As in Figure 5, these values are also close to each other, however, they now indicate the expected trend, i.e., a larger fibers content yields a larger ρ_{eff} at the TP. Furthermore, Figure 6 shows that the trendlines for larger fibers content (0.76%) are above those that correspond to the lower content (0.5%). I.e., for a given level of ρ_{eff} a larger fibers content causes a larger CLL (larger **n**/**m** ratios). Subsequently, the CLL at the transition point for the larger V_f is larger than that of the lower V_f, where **n**/**m** (at the TPs) = 1.7 and 1.5 (points B and A, Figure 6b), respectively.

This relative position of the two trendlines shows an additional observation: because minimum values of ρ_s (Figure 5) or ρ_{eff} (Figure 6) correspond to a single wide crack (**m** = 1) the corresponding CLL is equal to the total number of cracks (**n**/**m** = **n**/1 = **n**). Hence, based on the above observations, more cracks are formed for larger fiber contents. This result conforms to previous reported findings regarding the effect of using fibers on cracking control[31].

Another interesting point is that when the steel hardening is not considered the slope of the trend line's first branch reduces with the reduction of the fiber content (see Figure 5b). However, this change of the slope becomes much smaller when ρ_{eff} is taken into account, as shown in Figure 6b.

6 CONCLUSIONS

This paper presents an experimental study aimed to identify and quantify the cracking localization (CL) phenomenon in under-reinforced R/SFRC beams. Results of current experiments together with those of previous tests published by the authors were used for quantification of the cracking localization level (CLL) considering the effect of fiber content, V_f, and of longitudinal reinforcement ratio, ρ_s, over a wide range of ρ_s (0.15% to 3.3%) and the effect of rebar yield and ultimate strengths. The experimental program consisted of four-point bending tests of normal strength R/SFRC beam specimens with 400 and 500-MPa steel and fiber volumetric contents V_f of 0.5 and 0.75%. The CLL analysis was preceded by an extensive testing of notched beam specimens to classify the FRC mixtures, which yielded classes of 2.5d and 3d for the 0.5 and 0.76% mixtures, respectively.

A new definition is introduced for 'significantly wide cracks' that yields a unique definition of the CLL, when this phenomenon diminishes. Moreover, it is now proposed to change the definition of CLL and to use the ratio of the total number of cracks (formed prior to yielding) **n** to the number of 'significantly wide cracks' **m**. According to this definition, CLL increases when **n/m** increases and vice versa.

The study identified the existence of a transition point (TP), beyond which addition of fibers to the concrete mix do not affect CLL anymore.

The main observations from the experimental results are the following:

- CLL is more pronounced in R/SFRC beams with low longitudinal reinforcement ratios (ρ_s).
- For a given mixture and reinforcement ratio, the scatter of the measured CLL was larger at lower values of ρ_s.
- Consideration of only the amount of conventional tension steel without taking into account its stress hardening leads to non-physical trend of TP depending on V_f.
- Therefore, a new parameter $\rho_{eff} = \rho_s \cdot f_u/f_y$ is introduced, which considers both the amount and hardening of the conventional reinforcement.
- In terms of the new parameter, TP was larger for the mixture with the larger fibers content.
- Furthermore, for a given level of ρ_{eff} a larger fibers content causes a larger CLL (larger **n**/**m** ratios). Subsequently, the CLL at the TP for the larger V_f is larger than that of the lower V_f.
- The results are further supported by previous findings that establish that more cracks are formed for larger fibers contents.

The parameters introduced in this study represent both the amount and stress hardening of the tension steel. Note that the steel hardening should consider both stress and strain parameters. However, the current use of a simplified f_u/f_y parameter yields good results.

The use of the steel parameters enables a clear delineation of the cracking localization phenomenon in R/SFRC beams, where for low ρ_{eff} there are high levels of CLL. The importance of this finding refers to the reported decrease of flexural ductility in R/SFRC beams due to high CLL. Hence, the importance of the ability, achieved in the current findings, to quantify the conditions for TP's in various cases.

ACKNOWLEDGMENT

This work was partly supported by the Israeli Ministry of Immigrant Absorption (through a joint grant from the Centre for Absorption in Science and the Committee for Planning and Budgeting of the Council for Higher Education under the framework of the KAMEA Program).

REFERENCES

1. *fib*, Model Code for Concrete Structures 2010. Ernst & Sohn 2013.
2. R. D. Jordon, L. Seong-Cheol, and F. J. Vecchio, “Cracking Behavior of Steel Fiber-Reinforced Concrete Members Containing Conventional Reinforcement,” *ACI Struct. J.*, vol. 111, no. 1, pp. 93–102, 2014.
3. D. Redaelli and A. Muttoni, “Tensile behaviour of reinforced ultra-high performance fiber reinforced concrete elements,” *Concr. Struct. - Stimul. Dev. Proc. fib Symp. Dubrovnik 2007*, pp. 267–274, 2007.
4. A. N. Dancygier, Y. S. Karinski, and Z. Navon, “Cracking localization in tensile conventionally reinforced fibrous concrete bars,” *Constr. Build. Mater.*, vol. 149, pp. 53–61, 2017.
5. I. H. Yang, C. Joh, and B. S. Kim, “Structural behavior of ultra high performance concrete beams subjected to bending,” *Eng. Struct.*, vol. 32, no. 11, pp. 3478–3487, 2010.
6. A. N. Dancygier and Z. Savir, “Flexural behavior of HSFRC with low reinforcement ratios,” *Eng. Struct.*, vol. 28, no. 11, pp. 1503–1512, 2006.
7. D. Y. Yoo and D. Y. Moon, “Effect of steel fibers on the flexural behavior of RC beams with very low reinforcement ratios,” *Constr. Build. Mater.*, vol. 188, pp. 237–254, 2018.
8. D. Y. Yoo, Y. S. Yoon, and N. Banthia, “Predicting the post-cracking behavior of normal- and high-strength steel-fiber-reinforced concrete beams,” *Constr. Build. Mater.*, vol. 93, pp. 477–485, 2015.
9. A. N. Dancygier and E. Berkover, “Cracking localization and reduced ductility in fiber-

reinforced concrete beams with low reinforcement ratios," *Eng. Struct.*, vol. 111, pp. 411–424, 2016.

10. S. Werzbrger, Y. S. Karinski, and A. N. Dancygier, "Quantification of cracking localization in fibre-reinforced concrete beams," *IOP Conf. Ser. Mater. Sci. Eng.*, vol. 246, no. 1, pp. 1–6, 2017.

11. A. N. Dancygier and Y. S. Karinski, "Effect of cracking localization on the structural ductility of normal strength and high strength reinforced concrete beams with steel fibers," *Int. J. Prot. Struct.*, vol. 10, no. 4, pp. 457–469, 2019.

12. Tomislav Markic, Ali Amin, Walter Kaufmann and Thomas Pfyl, "Strength and Deformation Capacity of Tension and Flexural RC Members Containing Steel Fibers, ASCE, Journal of Structural Engineering, vol. 146: no. 5, pp. 04020069, 2020.

13. Schumacher P, Walraven JC, den Uijl JA, et al. (2009) Rotation capacity of self-compacting steel fibre reinforced concrete beams. *HERON* 54: 127–161.

14. A. N. Dancygier and Y. S. Karinski, "Probabilistic model of the crack localization in axially loaded fibrous reinforced concrete bars," *Eng. Struct.*, vol. 79, pp. 417–426, 2014.

15. Y. S. Karinsrki, A. N. Dancygier, and Z. Navon, "Experimental verification for a probabilistic model of fibers distribution along a reinforced concrete bar," *Mater. Struct. Constr.*, vol. 50, no. 2, pp. 1–10, 2017.

16. A. Bentur and S. Mindess, "Fibre Reinforced Cementitious Composites," vol. 10, no. 1, p. 53, 2006.

17. Gettu R, Gardner DR, Saldivar H, Barragan BE (2005), Study of the distribution and orientation of fibers in SFRC specimens. Mater Struct 38:31–37

18. M. G. Alberti, A. Enfedaque, and J. C. Gálvez, "A review on the assessment and prediction of the orientation and distribution of fibres for concrete," *Compos. Part B Eng.*, vol. 151, pp. 274–290, 2018.

19. B. Boulekbache, M. Hamrat, M. Chemrouk, and S. Amziane, "Flexural behaviour of

steel fibre-reinforced concrete under cyclic loading," *Constr. Build. Mater.*, vol. 126, pp. 253–262, 2016.

20. J. R. Deluce, S. Lee, and F. J. Vecchio, "Crack Model for Steel Fiber-Reinforced Concrete Members Containing Conventional Reinforcement," *ACI Struct. J.*, vol. 111, no. 111, pp. 93–102, 2014.
21. Yang Y, Walraven JC and den Uijl JA (2009) Combined effect of fibers and steel rebars in high performance concrete. *HERON* 54: 205–224.
22. A.N. Dancygier, Y.S. Karinski, RC beams with steel fibres - Towards better determination of their minimum conventional reinforcement ratio. fib Bulletin no. 95: Fibre Reinforced Concrete: From Design to Structural Applications. 2020: 246-253,
23. Y. Shao and S. L. Billington, "Predicting the two predominant flexural failure paths of longitudinally reinforced high-performance fiber-reinforced cementitious composite structural members," *Eng. Struct.*, vol. 199, p. 109581, 2019.
24. "Bekaert. Product data sheet 'Dramix RC-65/35-BN,'" p. 1200, 2005.
25. prEN 1992-1-1 (Draft), Eurocode 2: Design of concrete structures - Part 1-1: General rules - Rules for buildings, bridges and civil engineering structures. CEN, 2021
26. M. di Prisco, M. Colombo, D. Dozio · Fibre-reinforced concrete in *fib* Model Code 2010: principles, models and test validation, Structural Concrete 14 (2013), No. 4, 342-361
27. NF EN 14651+A1, "Test method for metallic fibre concrete - Measureing the flexural tensile strength (limit of proportionality (LOP), residual)," vol. 3, p. 17, 2012.
28. EN 206:2013+A1:2016, Concrete - Specification, performance, production and conformity. CEN, 2016
29. EN 1990:2002+A1:2005, Eurocode — Basis of structural design. CEN, 2010
30. M Di Prisco, G Plizzari, L Vandewalle , Fibre reinforced concrete: new design perspectives, Materials and Structures (2009) 42:1261–1281
31. L. Vandewalle, "Cracking behaviour of concrete beams reinforced with a combination of ordinary reinforcement and steel fibers," *Mater. Struct. Constr.*, vol. 33, no. 3, pp.

164–170, 2000.

32. T. Markić, A. Amin, W. Kaufmann, T. Pfyl, "Discussion on “Assessing the influence of fibers on the flexural behavior of reinforced concrete beams with different longitudinal reinforcement ratios” by Conforti et al. [structural concrete, 2020]", Structural Concrete (2021), 22(3), 1888-1891.

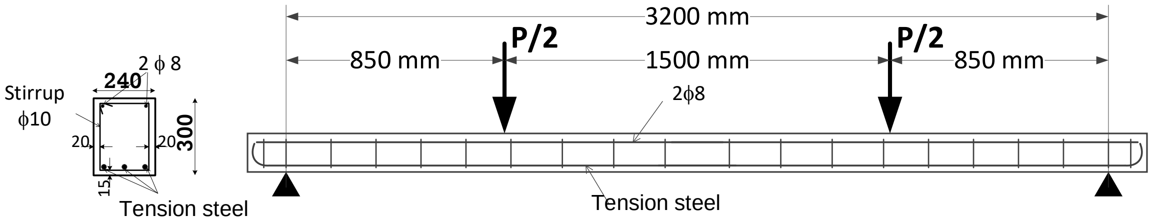

FIGURE 1 Scheme of tested beams.

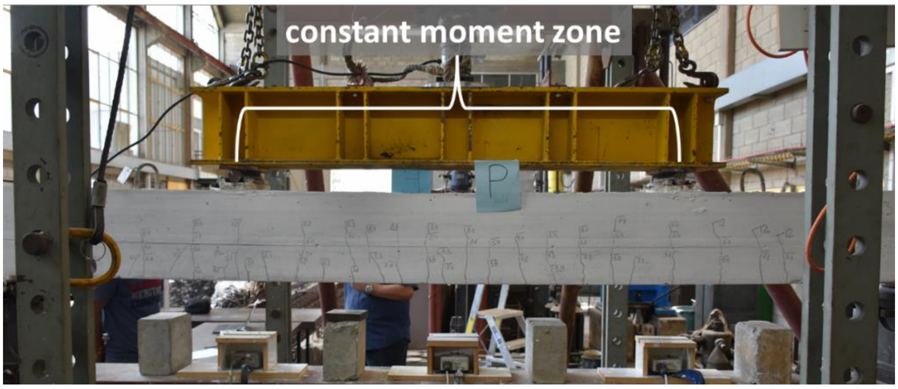

FIGURE 2 Specimen 60_053_3 just after yielding

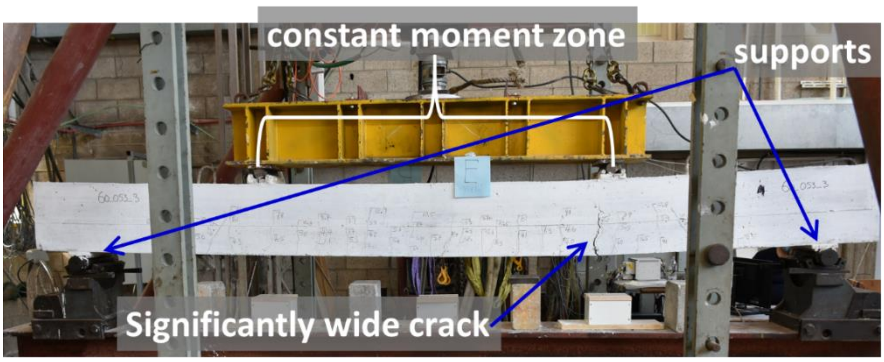

(a) Single wide crack

(b) Several wide cracks

(c) Most cracks are wide

FIGURE 3 CLL in the specimens at the end of the test

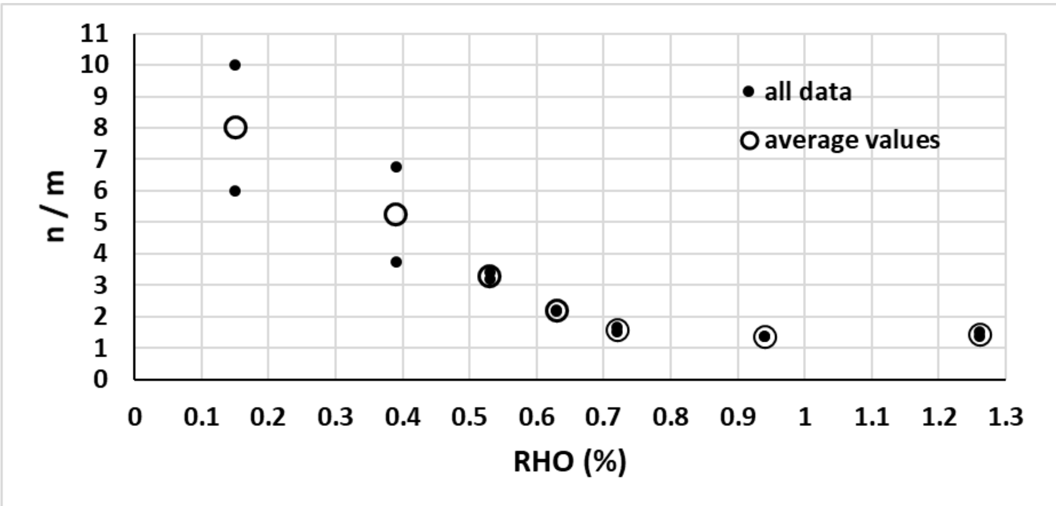

(a) V_f = 0.5% (c_f = 40 kg/m^3)

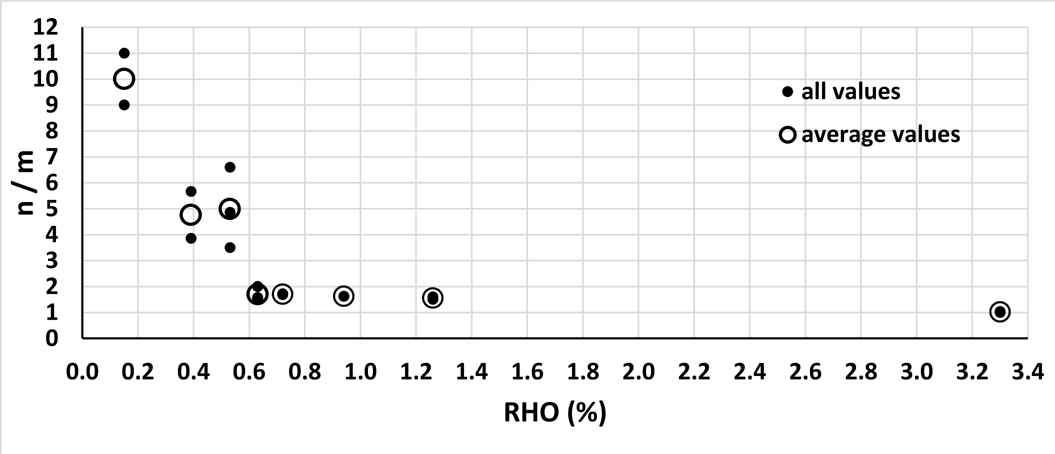

(b) V_f = 0.76% (c_f = 60 kg/m^3)

FIGURE 4 CLL vs. conventional reinforcement ratios

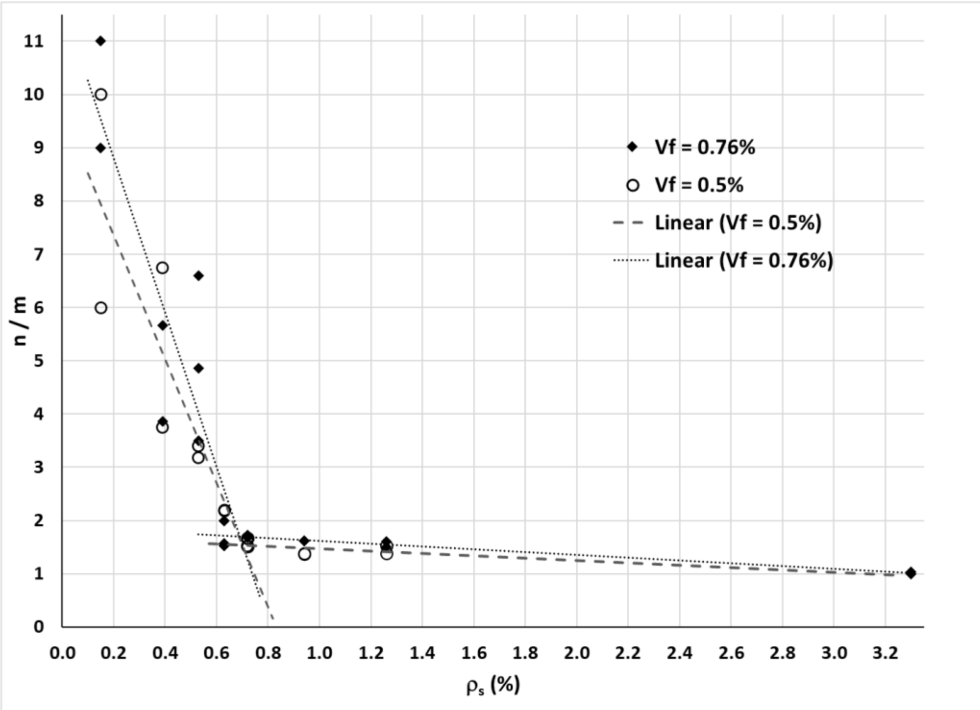

(a) Entire range of ρ_s

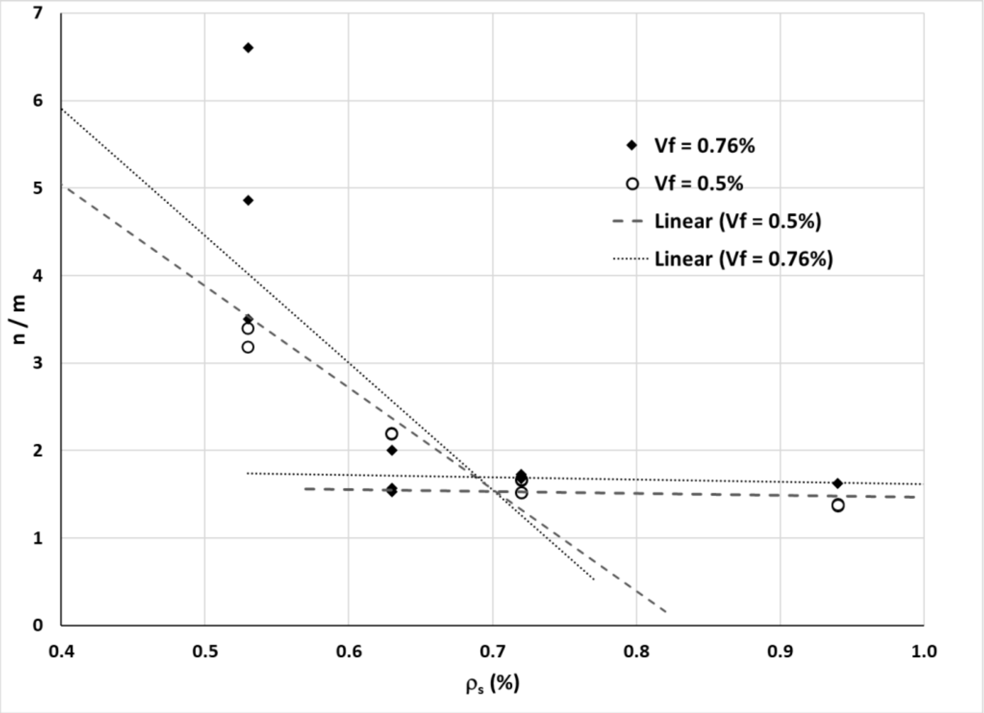

(b) Range of ρ_s in the proximity of the transition point

FIGURE 5 Transition point of the conventional reinforcement ratio ρ_s

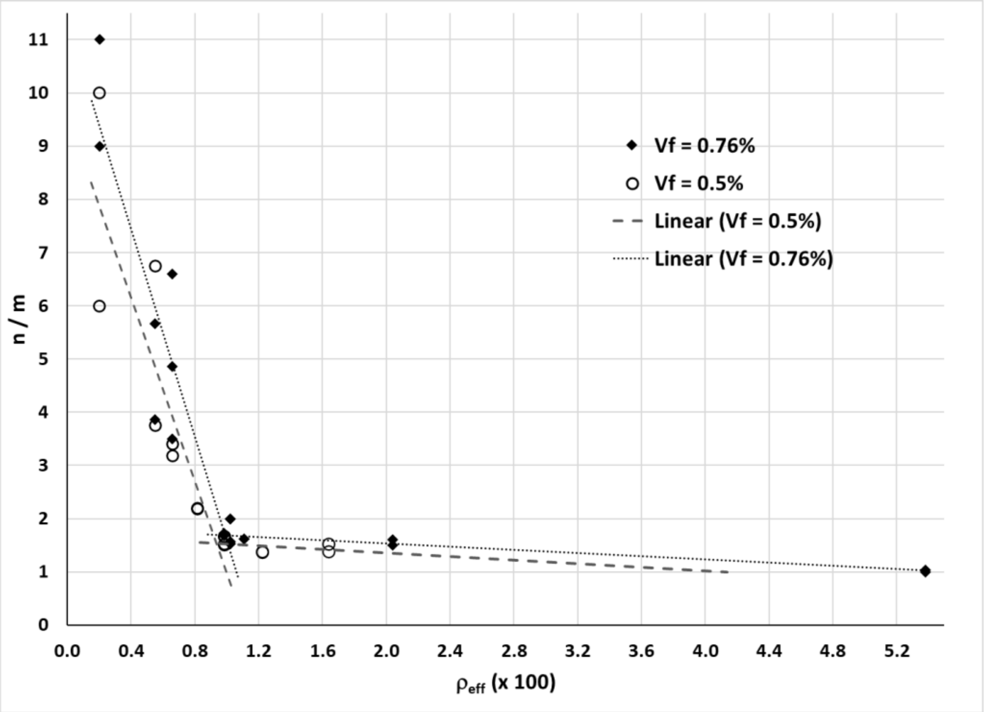

(a) Entire range of ρ_{eff}

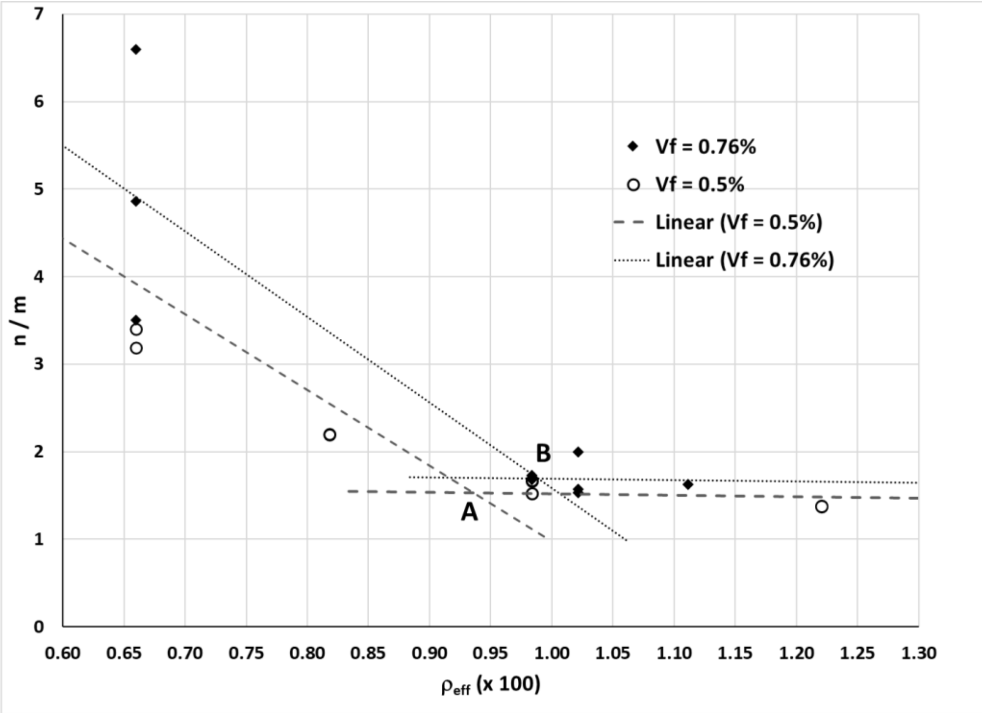

(b) Range of ρ_{eff} in the proximity of the transition point

FIGURE 6 Transition point of the conventional effective reinforcement ratio ρ_{eff}

Table 1. Details and notations of the R/SFRC specimens.

Test series	Specimen notation[1]	No. of speci-mens	Fibers		Tension reinforcement				f_c [2] (MPa)
			c_f (kg/m^3)	V_f (%)		ρ_s (%)	Measured strength (MPa)		
							yield	maxi-mum	
Previous	40-015	2	40	0.50	2ϕ8	0.15	503	677	30.9 (0.3)
	60-015	3	60	0.76			508	693	25.8 (1.0)
	40-039	2	40	0.50	2ϕ8 + 2ϕ10	0.40	409[3]	579[3]	30.4 (0.4)
	60-039	2	60	0.76					30.6 (0.2)
	60-063	3	60	0.76	2ϕ16	0.63	412	668	25.4 (0.5)
	60-094	2	60	0.76	3ϕ16	0.94	472	558	33.4 (0.5)
	60-126	2	60	0.76	4ϕ16	1.26	412	668	26.7 (1.4)
	60-330	2	60	0.76	5ϕ22	3.27	412	672	24.3 (0.9)
Current	40_053_1,2	3	40	0.50	3ϕ12	0.53	481	599	27.8 (0.57)
	40_053_3		40	0.50					29.8 (0.54)
	40_063_1,2	2	40	0.50	2ϕ16	0.63	529	687	33.7 (1.62)
	40_072_1,2	2	40	0.50	3ϕ14	0.72	423	578	29.3 (0.73)
	40_094_1,2	2	40	0.50	3ϕ16	0.94	529	687	30.6 (0.82)

40_126_1,2	2	40	0.50	4ϕ16	1.26	529	687	34.3(0.96)
60_053_1,2	3	60	0.76	3ϕ12	0.53	481	599	31.7 (1.43)
60_053_3		60	0.76					34.8 (0.63)
60_072_1,2	3	60	0.76	3ϕ14	0.72	423	578	29.1 (1.02)
60_072_3		60	0.76					30.2 (0.54)

{1} "40-" and "60-" denote 40 and 60 kg/m^3 fibers, respectively;
The last number (e.g., "015") denotes reinforcement ratio (%).
{2} Strength at 28 days, taken by 28 days wet-cured, 150-mm cubes;
Values in brackets denote standard deviations.
{3} Values are for 10-mm rebars

Table 1. Concrete mix components.

Test series	Water $\left[\frac{l}{m^3}\right]$	Cement $\left[\frac{kg}{m^3}\right]$	Sand $\left[\frac{kg}{m^3}\right]$	Aggregate $\left[\frac{kg}{m^3}\right]$	Fibers $\left[\frac{kg}{m^3}\right]$	WRA $\left[\frac{kg}{m^3}\right]$
Previous[11]	199 or 186	253	715	1147	0, 40, 60	1.52
Current	199	253	715	1147	40, 60	1.52

WRA= water reducing agent

Table 3. Residual strength f_{r1} and f_{r3} values

speci-men	1	2	3	4	5	6	7	8	9	10	11	12	13	14	15	16	17	18	19	20	21
0.5% (40 kg/m^3) fibers																					
f_{r1}	3.4	3.8	4.2	3.5	5.1	5.2	5	4.6	5.4	5.6	4.2	5.5	6.8	6.8	4.2	3.6	5.5	4.4	5.8	4	4.5
f_{r3}	3.2	4.5	4.4	3.6	4.4	5.8	5.4	4.8	5.6	6.1	4	5.9	7.4	7.4	4.5	4	4.3	4.5	4.9	3.7	4.6
0.76% (60 kg/m^3) fibers																					
f_{r1}	5.4	5.4	4.8	4.9	6.4	6.4	6.8	7.4	6.7	6.9	6.3	7.7									
f_{r3}	4.8	5.3	5.3	5.2	6.4	5.9	6.8	7	6.5	6.4	5.9	6.1									

Table 4. Mixtures classification

Mixture type	0.5% (40 kg/m^3) fibers	0.76% (60 kg/m^3) fibers
n	21	12
k_n	1.68	1.71
f_{r1m} [MPa]	4.81	6.26
σ_{r1m} [MPa]	0.98	0.94
CoV_1	0.20	0.15
m_{y1}	1.55	1.82
s_{y1}	0.20	0.15
f_{r1k} (Eq. (1)) [MPa]	3.36	4.79
f_{r1k} (Eq. (3) [MPa]	2.89	3.76
RSC	**2.5**	**3**
f_{r3m} [MPa]	4.91	5.97
σ_{r3m} [MPa]	1.13	0.69
CoV_3	0.23	0.12
m_{y3}	1.57	1.78
s_{y3}	0.23	0.12
f_{r3k} (Eq. (1)) [MPa]	3.27	4.86
f_{r3k} (Eq. (3)) [MPa]	2.94	3.58
f_{r3k}/RSC	1.18	1.19
RBC	**d**	**d**
Mixture classification	**2.5d**	**3d**

Table 5. Crack numbers (shaded cells refer to the previous test series)

Specimen notation	ρ_s (%)	ρ_f (%)	Number of cracks (average of two sides) **n**	**m**	CLL **(n/m)**	f_u / f_y (acc. to Table 1)
40_015_1	0.15	0.5	12	2	6.00	1.35
40_015_2	0.15	0.5	10	1	10.00	1.35
60_015_1	0.15	0.76	11	1	11.00	1.36
60_015_3	0.15	0.76	9	1	9.00	1.36
40_039_1	0.39	0.5	13.5	2	6.75	1.42
40_039_2	0.39	0.5	15	4	3.75	1.42
60_039_1	0.39	0.76	13.5	3.5	3.86	1.42
60_039_2	0.39	0.76	17	3	5.67	1.42
40_053_1	0.53	0.5	17.5	5.5	3.18	1.25
40_053_3	0.53	0.5	17	5	3.40	1.25
60_053_1	0.53	0.76	16.5	2.5	6.60	1.25
60_053_2	0.53	0.76	17.5	5	3.50	1.25

60_053_3	0.53	0.76	17	3.5	4.86	1.25
40_063_1	0.63	0.5	16.5	7.5	2.20	1.30
40_063_2	0.63	0.5	17.5	8	2.19	1.30
60_063_1	0.63	0.76	11	7	1.57	1.62
60_063_2	0.63	0.76	13	8.5	1.53	1.62
60_063_3	0.63	0.76	11	5.5	2.00	1.62
40_072_1	0.72	0.5	20	12	1.67	1.37
40_072_2	0.72	0.5	19	12.5	1.52	1.37
60_072_1	0.72	0.76	19	11	1.73	1.37
60_072_2	0.72	0.76	18.5	11	1.68	1.37
60_072_3	0.72	0.76	17	10	1.70	1.37
40_094_1	0.94	0.5	18	13	1.38	1.30
40_094_2	0.94	0.5	18.5	13.5	1.37	1.30
60_094_1	0.94	0.76	13	8	1.63	1.18
60_094_2	0.94	0.76	13	8	1.63	1.18
40_126_1	1.26	0.5	16	10.5	1.52	1.30
40_126_2	1.26	0.5	18	13	1.38	1.30
60_126_1	1.26	0.76	15	10	1.50	1.62
60_126_2	1.26	0.76	16	10	1.60	1.62
60_330_1	3.3	0.76	13.5	13	1.04	1.63
60_330_2	3.3	0.76	12	12	1.00	1.63

APPENDIX A – STRESS-STRAIN CURVES OF THE CONVENTIONAL REINFORCING BARS

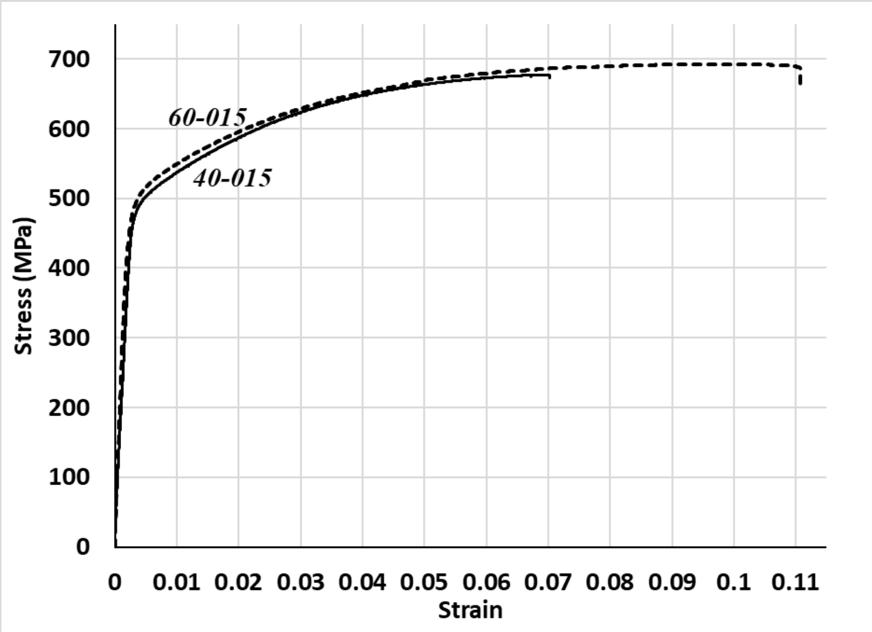

FIGURE A-1 8-mm rebars (averaged from 3 tested specimens for each test series)

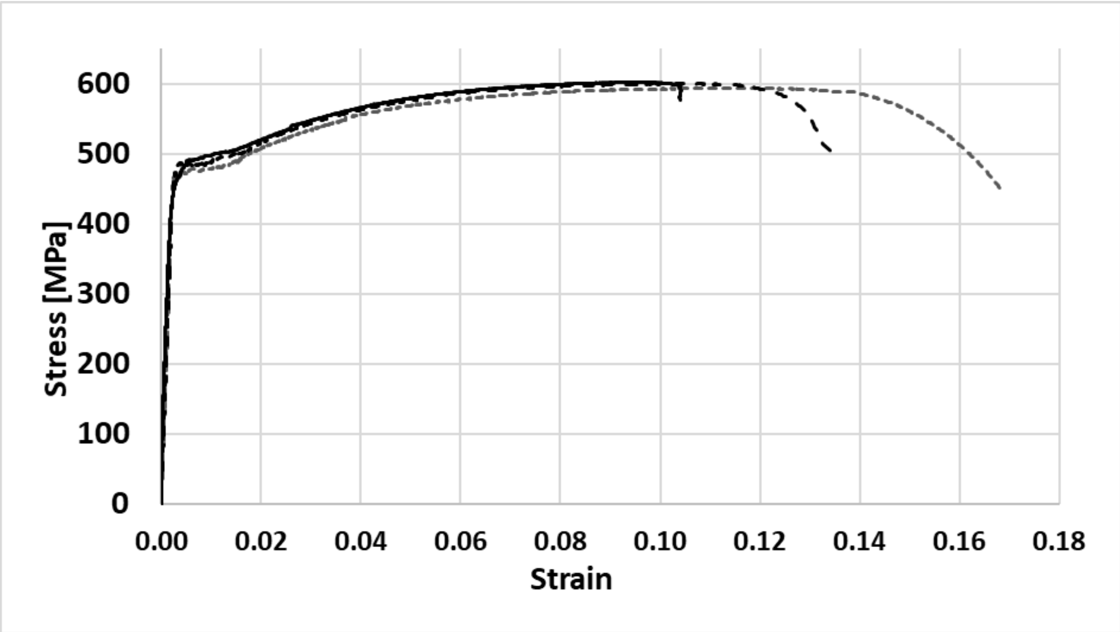

Figure A-2 12-mm rebars (3 specimens from 40-053 and 60_053)

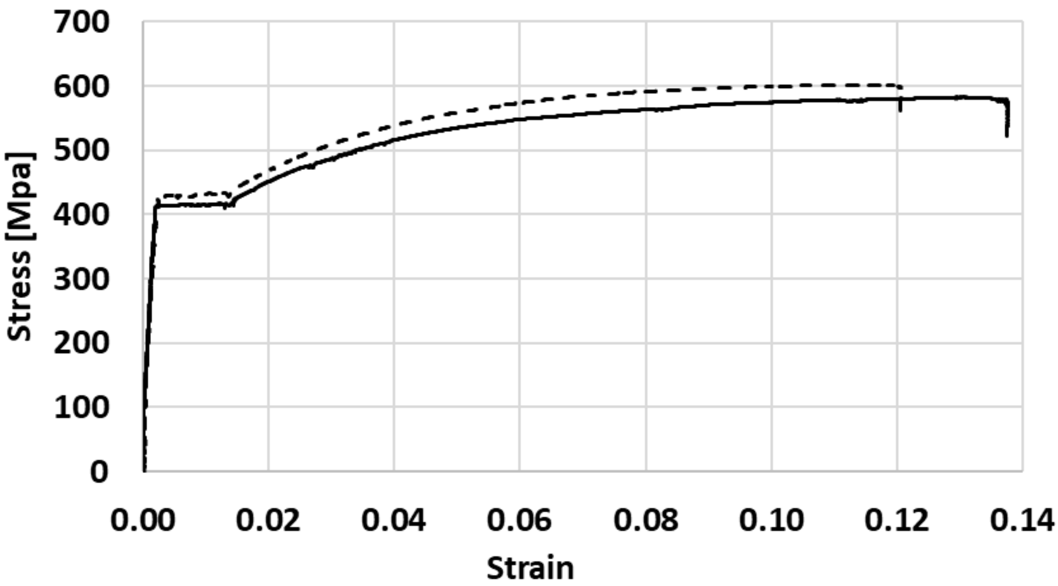

Figure A-3 14-mm rebars (2 specimens from 40-072 and 60_072)

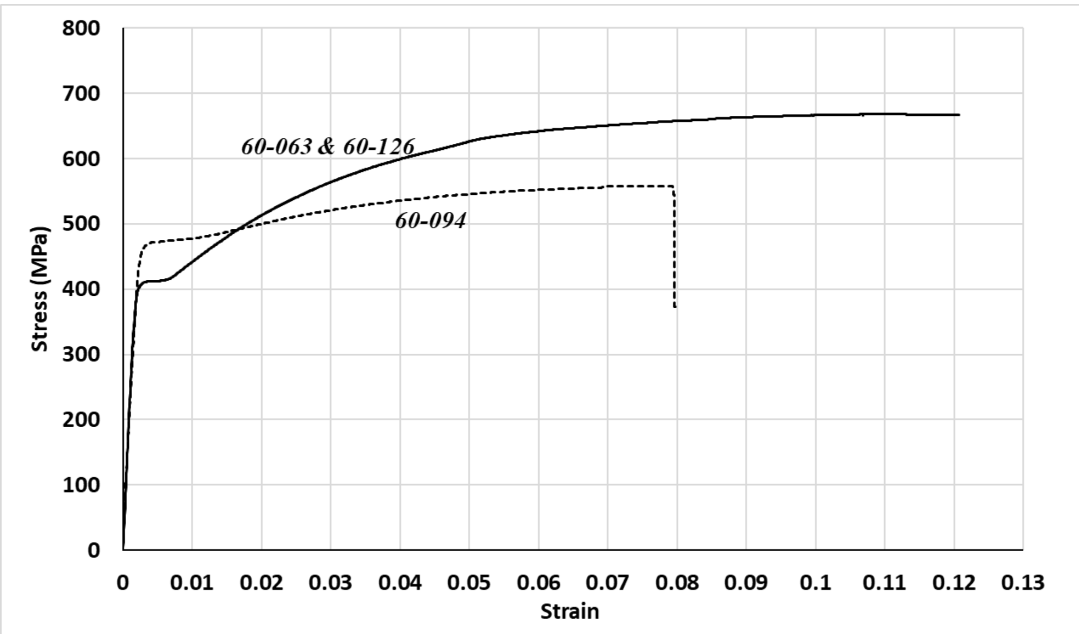

Averaged curves from 3 tested specimens for each test group or series

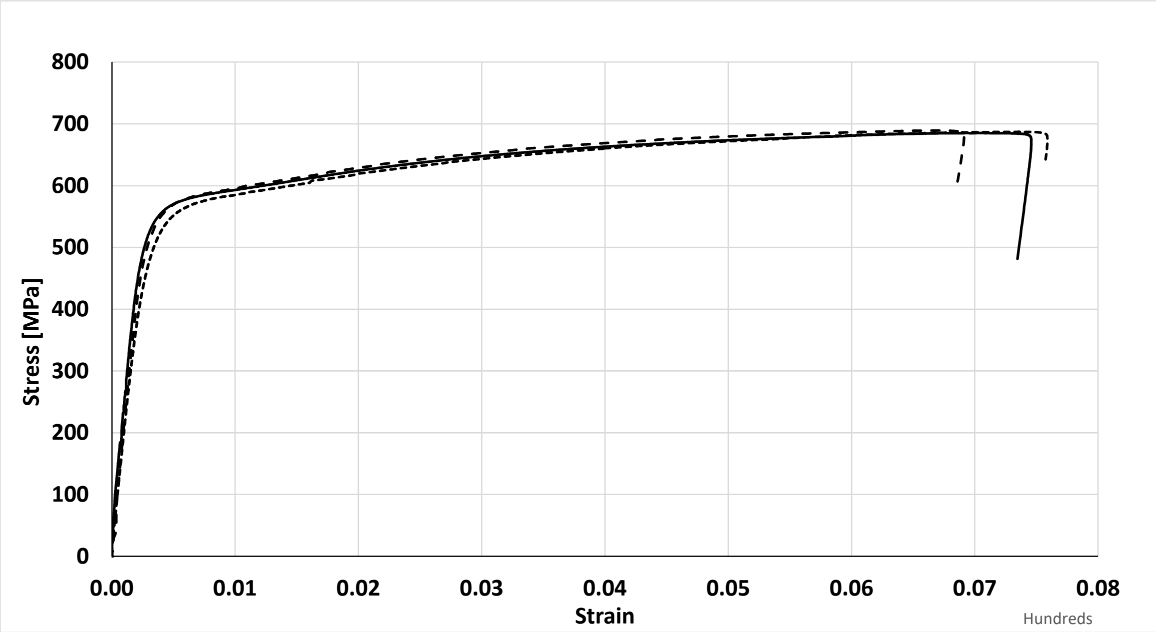

3 specimens from 40_063, 40_094 and 40_126

Figure A-4 16-mm rebars ()

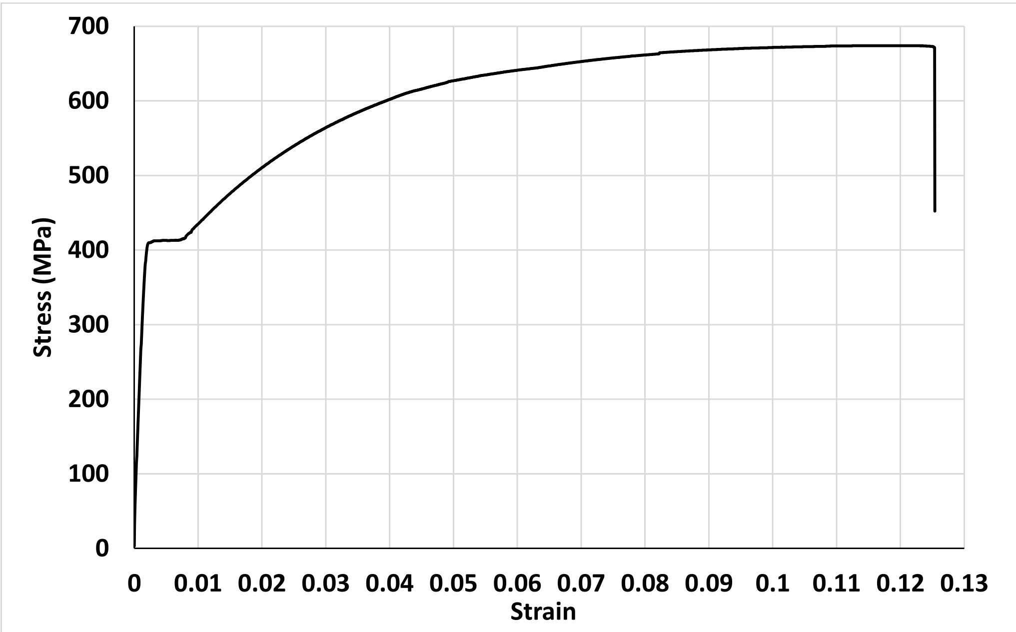

Figure A-5 22-mm rebars (averaged from 3 tested specimens for 60-330)

APPENDIX B - LOAD-CMOD CURVES OF NOTCHED BEAMS

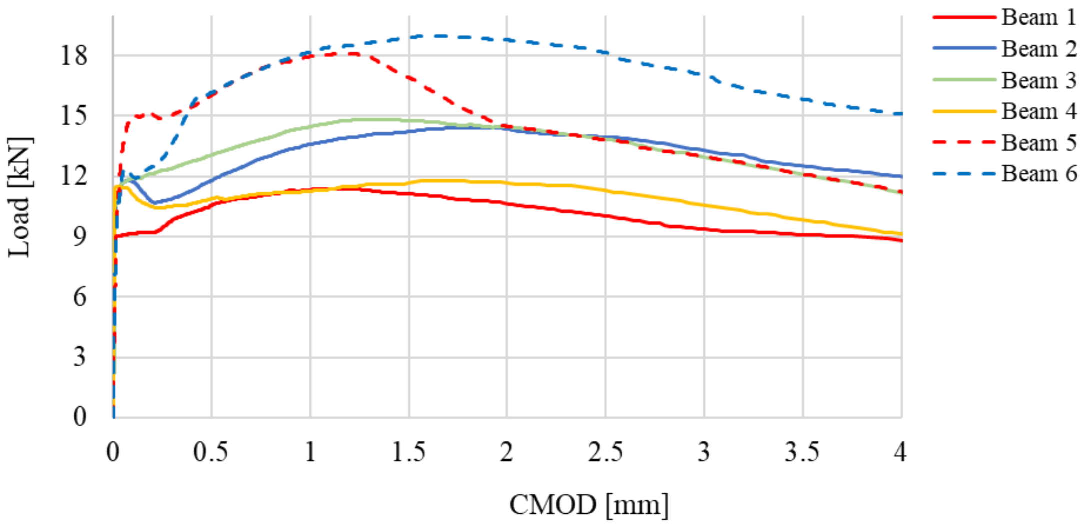

FIGURE B-1 Load-CMOD curves of notched beams of SFRC used in specimens 40_053 (dashed lines denote different casting at a later date).

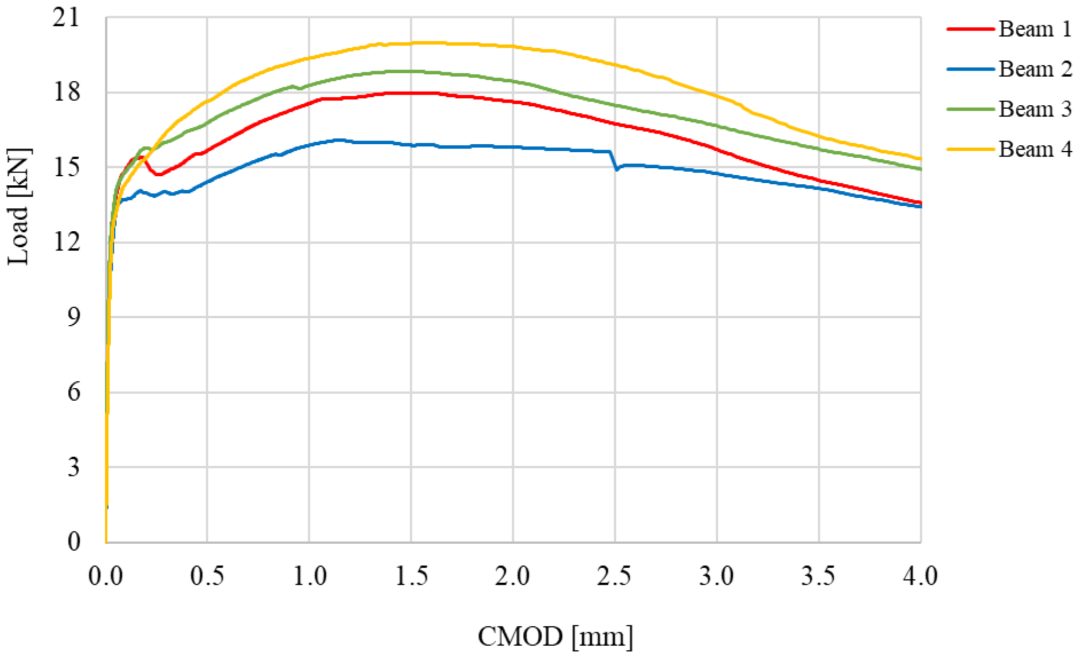

FIGURE B-2 Load-CMOD curve of notched beams of SFRC used in specimens 40_063.

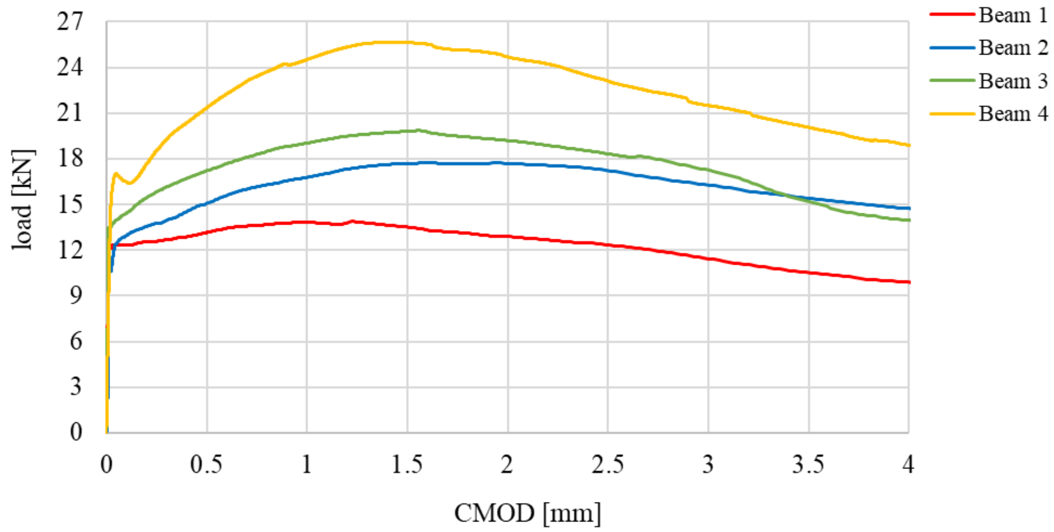

FIGURE B-3 Load-CMOD curve of notched beams of SFRC used in specimens 40_072.

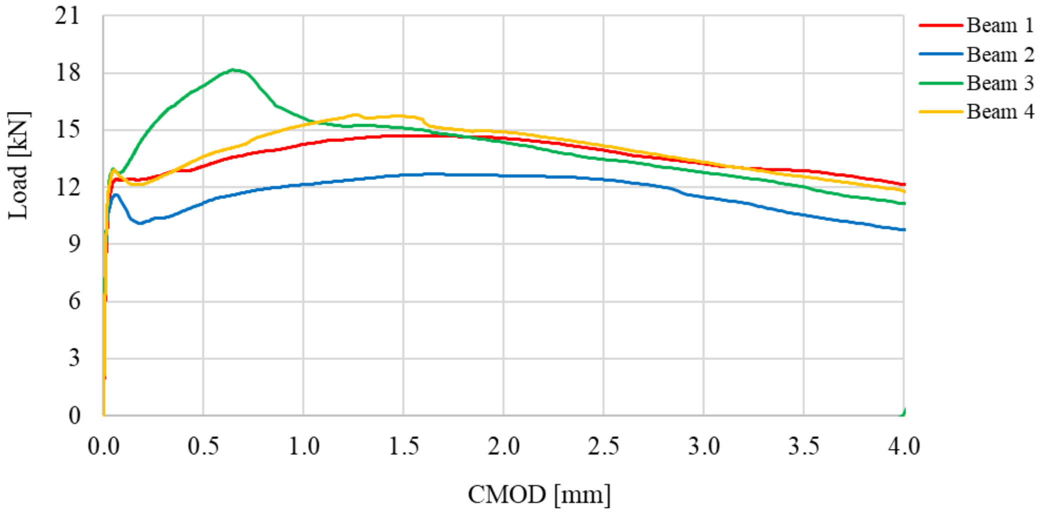

FIGURE B-4 Load-CMOD curve of notched beams of SFRC used in specimens 40_094.

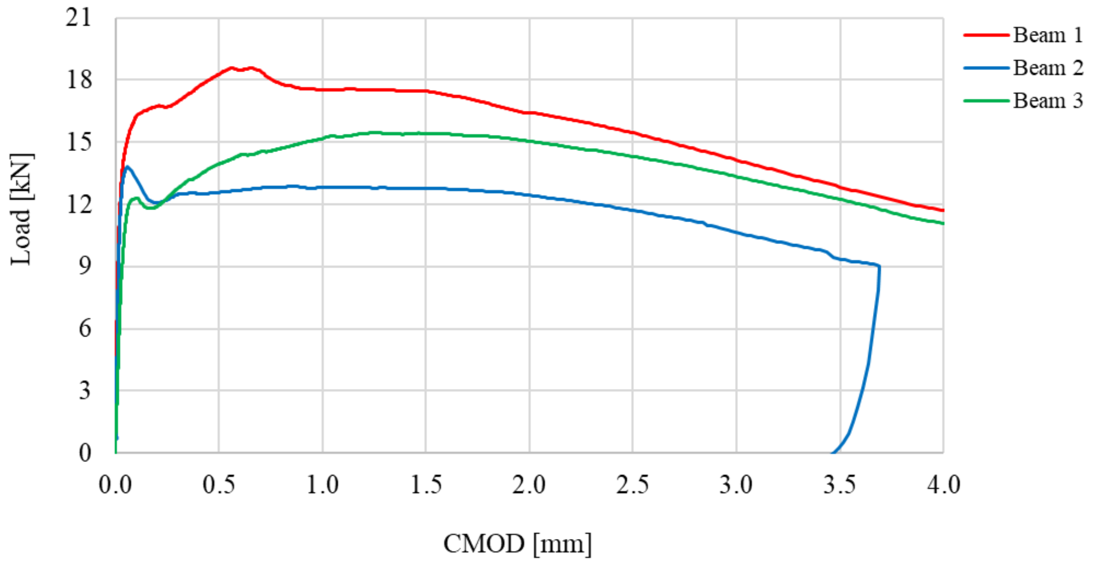

FIGURE B-5 Load-CMOD curve of notched beams of SFRC used in specimens 40_126.

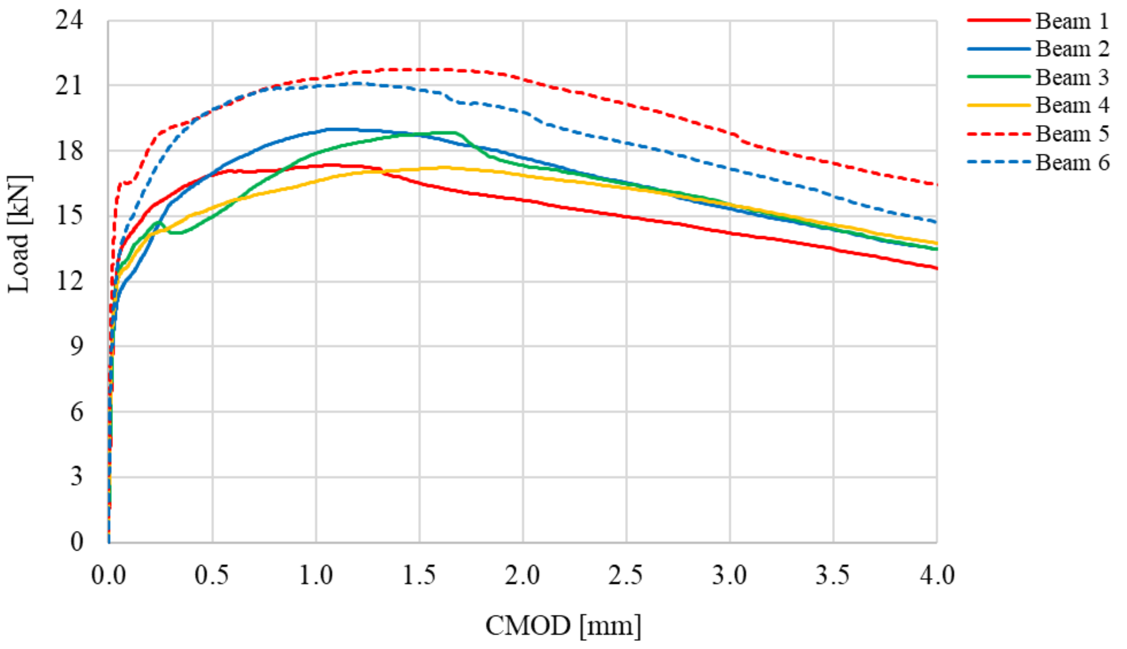

FIGURE B-6 Load-CMOD curve of notched beams of SFRC used in specimens 60_053 (dashed lines denote different casting at a later date).

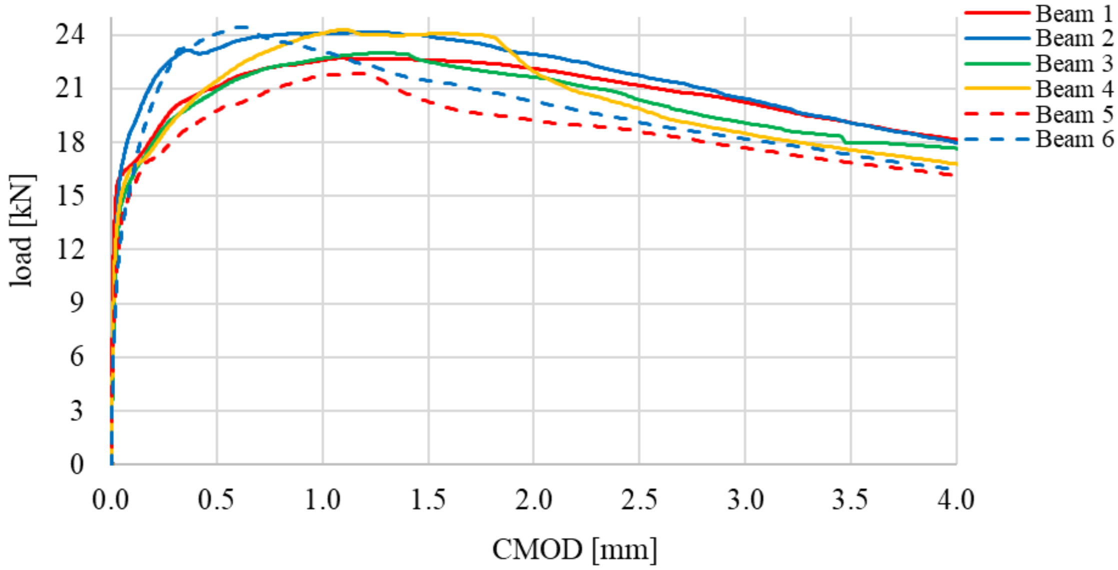

FIGURE B-7 Load-CMOD curve of notched beams of SFRC used in specimens 60_072.